

# ULTRA HEAVY COSMIC RAYS

P. H. Fowler, M. R. W. Mashedier, R. T. Moses, R. N. F. Walker  
and A. Worley

Department of Physics, University of Bristol

## INTRODUCTION

The existence in the cosmic rays of ultra-heavy (UH) nuclei with  $Z \geq 30$  was established by two separate experiments in 1966. Fleischer et al.<sup>(1)</sup> first demonstrated the fossil tracks of such nuclei in certain meteoritic crystals and shortly afterwards Fowler<sup>(2)</sup> established their existence in present-day cosmic rays with the detection of their tracks in photographic emulsion which had been exposed during a high altitude balloon flight. The fluxes of such nuclei are very low, only  $\sim 10^{-4}$  of that of iron, and the most suitable method of detection to date has been the analysis of the tracks formed by these particles in very large (several  $m^2$ ) arrays of plastic detector material, notably Lexan polycarbonate. Such exposures on balloons and on Skylab<sup>(3)</sup> have provided practically all present knowledge of the UH cosmic rays. Unfortunately, the charge resolution obtained was disappointing, even though scrupulous care was taken in the handling and etching of the material, and the charge scale itself of necessity had to be based on a considerable extrapolation from the iron peak and could not be used with great confidence. The situation now, however, is in the process of being transformed. We have two satellite experiments devoted to the study of UH cosmic rays and in operation at the moment. These are the Bristol University experiment on Ariel 6 launched on 3rd June 1979 and the joint group under Israel, Waddington and Stone on HEAO-C launched in September 1979. It is therefore appropriate, I believe, if I devote this review to the new preliminary results and a comparison of this material with the published data.

## THE BRISTOL ARIEL VI EXPERIMENT

The Ariel VI project offered the opportunity of a two-year exposure in orbit of a comparatively small counter experiment. The satellite was launched by NASA on the 100th Scout launch vehicle on 3rd June 1979 from Wallops Is., Virginia into a near-circular 625 km orbit inclined at  $55^\circ$ . The salient features of the detector, which is novel in a number of ways, are shown in Fig. 1. A spherical

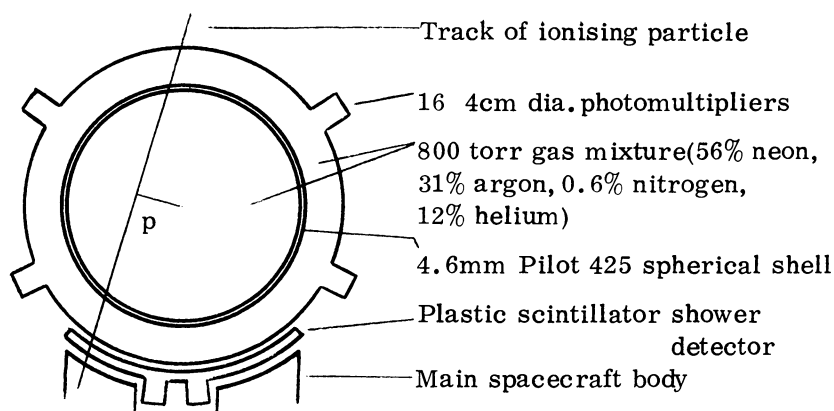


Fig. 1. Schematic cross-section of Ariel VI cosmic ray detector.

vessel of diameter 75cm contains a gas scintillation mixture and a thin spherical shell of Pilot 425 plastic, and forms a single optical cavity viewed by sixteen photomultipliers. The spherical symmetry of the detector has three significant consequences. It enables the detection of particles over the full  $4\pi$  steradians, although naturally in close Earth orbit the aperture is restricted, to about 8.5 steradians in this case. Secondly, the track geometry is characterised by a single quantity, the impact parameter  $p$ . Finally, the acceptance of all angles of incidence brings the important complication that the photomultipliers must of necessity intercept a fraction of the incoming particles; it is essential to remove such events from the data.

The passage of a typical cosmic ray nucleus results in the emission of Cerenkov radiation from each transit of the shell of Pilot 425 and scintillation from the whole path of the particle in the gas, which fills the space both inside and outside the shell. Both of these processes are well understood and the response of the detector should be accurately proportional to the square of the particle charge, except, perhaps, for the very highest charges along whose tracks electron recombination with the positive ion column can increase the scintillation yield. This effect of high ion density along the track, readily observable under laboratory conditions with fission fragments, will be discussed more fully in a later publication. The determination of the particle charge relies upon the estimation of each of the two components from the photomultiplier outputs. This can be achieved because the two components are emitted over markedly different timescales.

The gas is a mixture of argon, nitrogen, neon and helium with partial pressures as indicated in Fig. 1. The helium, included to facilitate ground leak tests, does not contribute materially to the light output. The scintillation consists largely of the band spectrum of nitrogen in the near ultra-violet, the nitrogen

being activated by excited argon states formed by the cosmic ray particle. Further argon excitations are contributed via excited neon states also formed by the cosmic rays. Both the scintillation and the Cerenkov emission fall largely in the absorption band of the Pilot 425 and are wavelength shifted to  $\sim 425\text{nm}$  and reradiated promptly and isotropically. This process is crucial in ensuring the near-homogeneous distribution of light within the cavity. The trapping within the shell by total internal reflection of the reradiated light is prevented by a lightly frosted finish on the outer surface. Any blue light has a lifetime in the optical cavity of  $\sim 20\text{ns}$ , which therefore dominates over the other timescales in the case of the Cerenkov emission. In contrast, the mean duration of the scintillation from the gas is  $\sim 300\text{ns}$ , which is largely due to the time for the excitation transfer from argon to nitrogen. The difference between these two timescales is significant and enables the proportions of each component in the composite Cerenkov/scintillation photomultiplier pulse to be determined. Measurements are made of the total light output and that part of the output received during a  $400\text{ns}$  gate which opens  $80\text{ns}$  after receipt of the fast leading edge of the Cerenkov pulse, and therefore contains little contribution from Cerenkov radiation.

In addition to the main sphere there is a plastic scintillator detector lying between the sphere and the main spacecraft body whose prime function is to flag those events with trajectories that pass through the spacecraft. This is necessary because an electron shower containing, say,  $N$  electrons can simulate the pulse due to a nucleus of charge  $\sqrt{N}$ , and can only develop when the products of a high energy nuclear interaction pass through several radiation lengths of matter. A study of the spacecraft had revealed several areas containing significant paths of high- $Z$  materials, in particular from the Ni-Cd battery and the considerable numbers of tantalum capacitors arranged in rows.

#### ESTIMATION OF CHARGE FOR INDIVIDUAL COSMIC RAYS

It is well known that a single pair of Cerenkov and scintillation measurements do not suffice for the individual determinations of  $Z$  and  $\beta$ , due to the double-valued nature of the Cerenkov/scintillation ratio. This occurs as a result of the relativistic rise in ionization at high energies. For the range of velocities up to  $\beta c \sim 0.99$ , however, which contains the major fraction of all events, the ratio is a monotonically increasing function of  $\beta$  and a solution is possible. In this velocity range the determination of  $Z$ ,  $\beta$  and  $p$  would therefore appear to require three independent measurements. The total and delayed signals introduced above represent the only two measurements available, yet a solution is possible in this detector since appropriate dimensions have been chosen for the inner and outer radii of the plastic shell so that  $\beta$  and  $p$  behave as far as possible as a single parameter. The major part of the uncertainty in the estimation of  $Z$  is not in the mismatching of the well-populated parts of the curves, but in the ambiguity associated with the relativistic rise. Thus the addition of a further optical cavity to make individual  $\beta$  and  $p$  determinations possible would not have addressed

itself to the major part of the problem. In any case, this course of action would have complicated this essentially simple experiment to an unacceptable degree so that it could not have matched the flight opportunity that was offered.

## RESULTS

We are reporting the results of our analysis of  $\sim 300$  days of real time and recorded data. The events on the experimental high priority store (HPS) have not yet been adequately evaluated but, due to irregularities in the tape recorder playback and command systems, should eventually provide a small amount of additional data. The live time that we cover here corresponds to an exposure of  $\sim 400 \text{ m}^2\text{sr days}$  for most events, an exposure of the same order as that of the Skylab plastic experiment. Our experiment has the advantage that it covers the full charge band  $Z > 32$  with nearly uniform efficiency. The choice of satellite altitude and orbital inclination has the result of exposing the detector to various regions where high fluxes of trapped radiation are found. The region of the South Atlantic Anomaly, where as expected the high flux of background protons severely disturbs the cosmic ray charge estimates, is excluded from all analyses. Occasional effects have also been observed in the southern auroral belt.

Charge estimates for all events are made on the basis of comparison of the total and delayed signals with those of iron nuclei. The  $Z = 26$  calibration is established for each day's data using about 10,000 iron peak events. No more frequent calibration is necessary, since the performance of all components of the experiment appears to be remarkably unchanging. The gas scintillation output, for example, has decayed by only 3% over the period covered here, and shows only a transient 7% fall during the  $14^\circ\text{C}$  temperature rise typically experienced by the detector sphere during an all-Sun period. This stability may be partly due to the low temperature ( $-18^\circ\text{C}$ ) at which the sphere is usually maintained.

The behaviour around and below the iron peak enables one to judge the resolution and interpret the high charge data. In any charge spectrum with good statistics the outstanding features are the skewness of the Fe and Ni peak and the dramatic fall in abundance of  $\sim 10^4:1$  between Fe and  $Z = 32$ . The relativistic rise at high energy produces the exponential tail to high  $Z$  and causes the Ni peak to appear only as a shoulder. Zn, with its much lower abundance of  $\sim 6 \cdot 10^{-4}$  of  $\text{Fe}^{(4)}$ , is smothered almost completely. The coefficient of the exponential tail is consistent with that expected for a particle energy spectrum of the form  $N(> E) \propto E^{-1.5}$  and the variation of the energy loss in the gas with particle energy. The values of  $\Delta Z$  due to this effect are proportional to  $Z$  and so dominate at the higher charges. The tail would still be serious even if the Poisson fluctuations were much reduced, and one would only gain considerably in resolution if the high energy particles could be individually recognised with certainty.

Fig. 2 displays the charge spectrum for events with apparent charge  $32 < Z_{\text{app}} < 50$  using the cut off restriction, cut off  $\geq 3\text{GV}$ . An odd-even effect

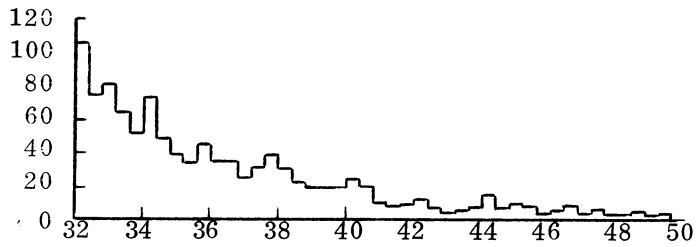


Fig. 2. Histogram of  $Z_{app}$  for  $32 < Z < 50$  and cutoff  $> 3GV$ .

is apparent throughout. The overall fall with increasing  $Z_{app}$  is enhanced by the tail from Ni and Zn. An odd-even effect is expected on the basis of our resolving power as determined on Fe, and indicates that these even nuclei are more common than their odd-numbered neighbours. However, significant abundance values of  $^{35}Br$  and  $^{37}Rb$  must be expected as they each have two stable or long-lived isotopes. Particularly prominent and therefore relatively abundant are  $^{38}Sr$  and  $^{44}Ru$ . Analysis of these measurements is considered in the next section.

A problem for the lower charges in this band results from the effects of the priority threshold, which was centred between 34.0 and 36.5 for practically all of the data. Only for  $Z_{app} > 37.5$  are events always given the highest priority whatever their geometry or velocity, and hence only for such particles is the recording efficiency unity throughout. For lower charges the recording efficiency is a strong function of both its charge and the instantaneous flux of nuclei with  $Z \geq 20$ .

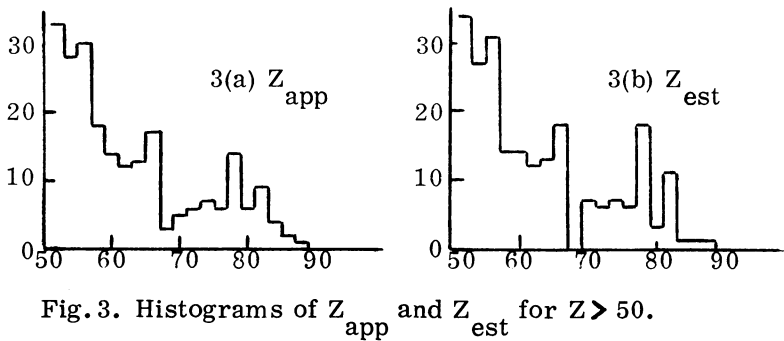


Fig. 3. Histograms of  $Z_{app}$  and  $Z_{est}$  for  $Z > 50$ .

The most interesting results, as expected, come in the highest charge band. Fig. 3a displays the histogram of apparent charge plotted in bins of width  $\Delta Z_{app} = 2.0$  charges, a figure we consider appropriate to the errors of charge assignment which are largely due to the effects of high energy particles. In Fig. 3b the events have been rebinned to produce the histogram for our best estimate  $Z_{est}$  of the actual charge of the particles by removing the effects of the



The spectrum of Fig. 3b can be compared directly with that from Skylab and with balloon data as is shown in Table 1. Points (b), (c) and (d) above are manifest in both of these other sets of data, but the Skylab estimate for  $Z \sim 63$  was considered by the authors to be uncertain, owing to the rapidly changing efficiencies near the threshold of the plastic, Lexan. The agreement thus supports the Lexan charge scale employed in the Skylab and balloon experiments.

## THE CHARGE SPECTRUM AT THE SOURCES

A particularly simple form of the 'leaky-box' model can explain many abundance features for  $Z \leq 26$  very adequately; it is appropriate to see whether such a model may apply to the UH cosmic rays as well. For this model we suppose that the sources of the cosmic rays are essentially uniformly distributed and that the

cosmic rays themselves are contained in a volume that contains interstellar hydrogen. We ignore energy loss by ionisation and take a value for the escape mean free path  $X_0 = 5 \text{gcm}^{-2}$ . In Table 2 we give the detected spectrum and the computed secondary and source spectra. Also shown is the abundance spectrum for the solar system from Cameron, 1973<sup>(6)</sup>. The tabulation shows that, with the exception of the highest charges with  $Z \geq 78$ , a substantial fraction of observed UH nuclei are in fact secondaries from interactions in interstellar space. This unfortunately hinders the detection of source features, as the proportions of true primaries are rather small. This arises because the interaction lengths involved fall in the range  $1 \leq \lambda_Z \leq 2 \text{gcm}^{-2}$  compared with the adopted value for the escape mean free path,  $X_0 = 5 \text{gcm}^{-2}$ . Although any lower value of  $X_0$  would be equally consistent with the UH data, higher values would result, for some charges, in negative source abundances.

## DISCUSSION

A natural charge spectrum with which to compare the cosmic ray results, and thereby hopefully gain insight into the conditions at the sources, is the solar system composition of Cameron. Earlier authors<sup>(7, 8)</sup> have made such a comparison for UH cosmic ray plastic track data and have concluded that the source appears to be enriched in the material which has undergone nucleosynthesis by the rapid neutron capture process. The apparent flux of actinides ( $Z \geq 90$ ), which can only be made by such an r-process, gave some support to this view. More recently, however, it has been suggested<sup>(9)</sup> that, at least for the elements  $3 \leq Z \leq 26$ , the cosmic ray source spectrum could be simply explained as a sample of normal interstellar material, modified only by the effects of differing ionization potentials for the various elements. The solar system composition is taken, in the absence of better data, as the required interstellar composition. In the light of our new data, we should consider whether this simple and attractive model could also apply to the UH nuclei, or whether enrichment in say r-process material is needed to explain the data.

TABLE 2  
Present Experiment

Charge	$N_{app}$		$N_{est}$	$N_{sec}$	$N_{source}$		Cameron Solar System Abundances
	(a)	(b)					
26	$2.4 \times 10^6$	$5.0 \times 10^6$	$5 \times 10^6$	$5 \times 10^6$	$10^6$		$10^6$
32				290			170
34	315		590	220	88 ± 12		92
36	183		330	144	46 ± 8		68
38	156		315	97	55 ± 8		39
40	95		180	60	32 ± 7		37
42	43		66	48	5 ± 5		5.6
44	44		94	40	15 ± 5	} 26 ± 4	2.5
46	33		63	25	11 ± 4		2.1
48	21		37	22	4.5 ± 4	} 4.8 ± 3	2.2
50	16		30	29	0.3 ± 4		4.6
52		33	34	17	5.6 ± 3.1	} 13.8 ± 3.9	8.5
54		28	27	17	3.2 ± 2.6		7.3
56		30	31	16	5.0 ± 2.6		6.2
58		18	14	6	2.8 ± 2.0	} 5.0 ± 1.6	1.8
60		14	14	8	2.2 ± 1.7		1.03
62		12	12	10	0.7 ± 1.7	} 6.2 ± 1.9	0.31
64		13	13	9	1.4 ± 1.7		0.44
66		17	18	5	4.1 ± 1.8		0.52
68		3	-2	4	-1.6 ± 1.5	} < 2.0	0.34
70		5	7	4.6	0.6 ± 1.6		0.30
72		6	6	5.4	0.3 ± 1.6		0.30
74		7	7	3.2	1.5 ± 1.6	} 8.6 ± 2.7	0.23
76		6	6	4.5	0.6 ± 1.6		1.36
78		14	18	2.7	6.5 ± 2.4		2.2
80		6	3	1.9	0.4 ± 1.6	} 5.7 ± 1.8	0.7
82		9	11	0.7	4.4 ± 2.0		5.0
84		4	1	0.1	0.5 ± 1.2		0.1
86		2	1	-	0.5 ± 0.8	} 2.0 ± 1.2	-
88		1	1	-	0.5 ± 0.5		-
≥ 90		2	2	-	1.0 ± 0.7		0.10

The figures listed in columns (a) and (b) for  $N_{app}$  refer to the actual numbers of events used for the determination of the charge spectrum. Column (a) uses data for geomagnetic cutoff values greater than 3.0GV only. Column (b) uses all data. The errors shown are due to Poisson statistics alone and are quite strongly negatively correlated in adjacent charge bins. Thus wider bins are used at higher charges to display the features of the source spectrum.

The comparison between the source spectrum and the solar system abundances may be summarised as follows:

- (a) the UH component as a whole has an abundance, when normalised to iron, close to that of the solar system. This has long been apparent and is again present in the results of this experiment. The total fluxes in the bands of charge  $34 < Z < 50$  and  $Z > 50$  each fall within a few percent of the solar system figures, in the latter case being based on 230 observed events. The low fluxes we observe in the actinide and  $Z \sim 70$  regions are also what would be expected if the two spectra had a common origin. The 18 events around  $Z \sim 70$  in the raw data appear to be spallation products.
- (b) the main features of the solar system composition are the two peaks around  $Z = 54$  and  $Z = 80$  corresponding to neutron closed shells at production with  $N = 82$  and  $126$ , respectively. We would expect, on the basis of the model, to see these in the cosmic ray source and indeed, they are both clearly present. The ratio between the abundances in the two peaks, however, differs markedly from the solar system value, showing a preference for the higher charges. For the ratio  $\frac{52 \leq Z \leq 56}{74 \leq Z \leq 84}$  we obtain  $0.95 \pm 0.3$  compared with the solar system value of  $2.5$ .
- (c) the solar system abundances would lead us to expect a particular distribution within each peak; in the case of the lower peak, a fairly uniform distribution, and for the peak around  $Z = 80$ , a preference for lead ( $Z = 82$ ) rather than platinum ( $Z = 78$ ). Our results indicate that the upper peak is predominantly platinum. The Pt/Pb ratio of  $1.5 \pm 0.7$ , which has survived nearly unchanged from the raw data, is to be compared with the solar system value of  $\sim 0.45$ . In the case of the lower peak we can present no evidence that the distribution is other than similar to that of the solar system.
- (d) the most striking abundance anomalies occur at charges  $Z \sim 44$  and  $Z \sim 64$ . In each region, the cosmic rays are approximately five times overabundant when compared with the solar system.

The overabundances at  $Z \sim 44$ ,  $64$  and  $78$  are not explainable with the simple model with solar system abundance values. They can, however, all be considered as supporting the evidence for an enrichment in r-process nuclei first suggested by the passive data. This interpretation of the anomalies at  $Z \sim 44$  and  $64$  requires elaboration. It is noteworthy that both of these charge regions, which correspond to two mass regions around  $A=105$  and  $A=164$ , are the sites of small solar system abundance anomalies. A number of authors have advanced explanations for these solar system features in terms of contributions from fission fragments. The feature around  $A=105$  is interpreted by Ohnishi<sup>(10)</sup> as due to the lighter fission fragments from  $\beta$ -induced and spontaneous fission in the source during the final phase of r-process nucleosynthesis. The parent nuclei have a wide range of masses around  $A=250$ , but since the mass of the lighter fragment is very nearly independent of that of its parent the feature at  $A \sim 105$  remains relatively sharp. For the heavier peak centred on  $A=164$ , which is both broader and more pronounced, Steinberg and Wilkins<sup>(11)</sup> invoke fission of superheavy

elements with  $A \sim 300$ . This is a higher mass than would be associated with the closed shell and abundance peak with  $N=184$ ,  $Z=94$  during the r-process, because these authors consider that such nuclei would tend to decay to two fragments with mass ratio close to unity, rather than the familiar asymmetric decay which occurs at other masses. The observed feature is produced by the more massive fragments from fission of a relatively narrow band of parent masses.

In the cosmic ray source each of these peaks is overabundant and approaches  $10^{-5}$  of the flux of iron nuclei, a figure comparable with the main peak at  $Z \sim 78$ . Thus, if explained in terms of fission, the source abundance of the transuranic species would need to be at least of this magnitude. Such a figure is consistent with models involving a cyclic r-process in which the number of neutrons per seed nucleus and the r-process duration are together sufficient not only to raise the masses of the seed nuclei to high values, at which point they undergo fission, but also to allow their daughter fragments to repeat the process. In such models (see, for example<sup>(12)</sup> and <sup>(13)</sup>) the peak centred at  $N=184$  accumulates an abundance comparable with that of the peak at  $N=126$ , which produced the platinum feature. The accompanying amount of material with  $A \sim 300$  synthesized in the same process is thought to be small, and thus any explanation of our abundance anomalies in terms of a significant contribution from nuclei with  $A \sim 300$  would raise the problem of accounting for the presumed even higher abundance of nuclei with  $A \sim 280$ . The combined abundance of Xe, Ba and Ce enables an upper limit of  $\sim 1.5 \cdot 10^{-5}$  of Fe to be placed upon the size of the abundance peak at  $N=184$ ,  $A=280$  in such circumstances, if all these nuclei are ascribed to fission fragments, this figure is little greater than that suggested by the rare earth abundance feature. It is thus perhaps attractive to consider the  $N=184$  abundance peak itself as the source of the main anomalies, the original mass of 280 being distributed between two peaks at  $A=105$  and 164 and about ten neutrons. This, of course, would be contrary to the views of Steinberg and Wilkins (*ibid*) who consider that fission will be nearly symmetric for these nuclei.

The present best estimate of the flux of cosmic ray nuclei with  $Z \geq 90$  comes from the Skylab data summarised in Table 1. On this basis we would expect to have observed four such events in our present sample. Two highly charged particles were detected with  $Z_{app} = 98$  and 114 although at this stage, clearly, neither event should be taken wholly at face value. The event with  $Z=98$  could be a perfectly normal actinide. Its light was well distributed in the main sphere and there was no accompanying signal from the plastic scintillator. The highest charge event, however, did activate the plastic scintillator detector and accordingly its interpretation as an electron shower cannot be excluded.

Finally, we must consider the source spectrum for charges in the range  $32 \leq Z \leq 42$ . As already noted, their general abundance is similar to that of solar system material. In this charge band the balloon-borne counter experiments of Israel et al. (*ibid*) provide the best existing source of data. Table 3 shows abundance values from Israel, the present experiment and the solar system.

TABLE 3

Charge	Present Experiment		Israel et al. 1979	Cameron Solar System		H. B. S.
	Detector	Source		All	r-process	
26	$10^6$	$10^6$	$10^6$	$10^6$	$10^6$	
28	$5 \cdot 10^4$	$5 \cdot 10^4$	$5 \cdot 10^4 \pm 4\%$	$5.8 \cdot 10^4$	0	
29	-	-	-	650	0	
30	-	-	$600 \pm 100$	1500	0	1500
31	-	-	$103 \pm 35$	58	0	41
32	-	-	$94 \pm 33$	138	0	106
33	-	-	$39 \pm 12$	8	0	2.4
34	$118 \pm 8$	$88 \pm 11$	$33 \pm 12$	80	34	36
35	-	-	$44 \pm 15$	16	9	1.3
36	$67 \pm 6$	$46 \pm 8$	$34 \pm 12$	65	11	20
37	-	-	$23 \pm 11$	7.1	3.6	2.1
38	$64 \pm 6$	$55 \pm 8$	$33 \pm 13$	32	0.9	27
39	-	-	$5 \pm 5$	6.0	1.6	1.7
40	$36 \pm 5$	$32 \pm 7$	$16 \pm 9$	34	8.4	4.7
41	-	-	-	1.7	1.0	0.0
42	$13 \pm 4$	$5 \pm 5$	-	4.8	1.3	0.4
Based on 730 events $Z \geq 33$			54 events $Z \geq 31$			

Table 3 gives comparisons between the present experiment and the existing balloon data of Israel et al. for the lower charges. Also shown are Cameron's abundance values and separately those from the r-process alone. The final column shows a computed H. B. S. spectrum normalised at Zn.

There is general agreement between the two sets of cosmic ray data, but in our results  $Z=32$ , which is marked in Israel's data, does not appear strongly, although it may be partially masked by the relativistic rise tails of Ni and Zn. Our results show that all the even charges  $34 \leq Z \leq 40$  are important in the source spectrum, with  $Z=34$  the most abundant, and that compared with the solar system,  $Z=38$  is somewhat enhanced in the cosmic rays. There is a rapid fall for  $Z > 40$ .

Models of r-process nucleosynthesis in which parameters are chosen to fit the high charge data do not normally produce these lighter elements with  $A < 78$ . An exposure to a far smaller integrated neutron flux is required to make nuclides of mass  $58 \leq A \leq 76$ . This avoids the otherwise rapid build-up to the closed shell at  $N=50$  due to the prompt capture of neutrons without intervening  $\beta$ -decays, by the Fe seeds, which produces a marked peak in the region of  $A=80$  but very little material with lower mass. The strength of the feature associated with  $N=50$  is, however, model dependent. If, for example, more seed nuclei are continuously introduced the peak remains strong. If not, then the whole feature can wither as the nuclides undergo  $\beta$ -decay and capture further neutrons. Clearly, therefore, one or more additional processes must be involved in the production of nuclides in the range  $58 \leq A \leq 76$  both for the cosmic ray source and for the solar system material.

From a study of abundance values from the balloon data of Israel et al.<sup>(4)</sup>, Wefel, Schramm and Blake<sup>(14)</sup> concluded that a form of the s-process that occurs

in massive stars, the helium burning s-process (HBS) may well be significant in this charge region. This process meets the requirement for a limited neutron exposure introduced above. The authors drew attention to the fact that these massive stars are the supernova progenitors. Thus, if supernovae are the source of the bulk of the galactic cosmic rays, material made in the HBS might be expected to be present in significant quantities in the cosmic rays. Furthermore, such stars are also the source of the abundant Fe that pervades the galaxy and solar system and is also such an abundant and important constituent of the cosmic ray source. No less than 5% of the total mass (and energy) of the cosmic rays is contributed by Fe nuclei, which are considerably overabundant when compared with hydrogen.

Comparison of the cosmic ray spectra in Table 3 with solar system abundance values shows a high level of agreement between the two sets of data. However, when compared with the r-process contribution alone the fit is poor, not only for  $Z=32$  as expected, but also for  $Z=38$ . This species is prominent in our source spectrum but is almost by-passed by the r-process, since there is only one accessible nuclide,  $^{88}_{38}\text{Sr}$ . In addition, the prominence of the peak at  $Z=34$  is not matched in the experimental data. The HBS process on its own is expected to be responsible for a considerable fraction of the solar system material for the range  $32 \leq Z \leq 40$  and its normalization is usually fixed by demanding that it be responsible for all  $^{58}_{26}\text{Fe}$ . Since the abundance of cosmic ray  $^{58}_{26}\text{Fe}$  is not well-known, we can instead choose to normalise to, say, cosmic ray Zn. Such a spectrum is given in Table 3. Noteworthy features are the strong odd-even effect, rather similar abundances for the even nuclei with  $Z=34, 36$  and  $38$ , and the rapid fall-off in abundance for  $Z \geq 40$ . On its own the HBS yield has strong similarities to the cosmic ray source spectrum for  $30 < Z < 40$ , but the best fit is to the mix represented by the solar system, which contrasts to the situation for  $Z > 50$ .

## CONCLUSION

The Ariel VI experiment provides for the first time data of reasonable statistical weight over the entire band of UH cosmic ray nuclei. Comparison of the measured and source abundances are made with solar system material. There are striking similarities and equally striking divergences. The production of nuclides of the solar system and of the cosmic rays both appear to require a number of processes of nucleosynthesis. However, it seems clear that the mix of processes involved has to be substantially different for the two types of material, and the cosmic ray source appears rich in r-process material that is believed to be synthesized in supernova explosions. As new data become available from the satellite experiments, so important advances in understanding can be expected in the near future.

## REFERENCES

1. Fleischer, R.L., Price, P.B., Walker, R.M., Maurette, M., and Morgan, G.: 1967, *J. Geophys. Res.* 72, pp. 355-366.
2. Fowler, P.H., Adams, R.A., Cowen, V.G., and Kidd, J.M.: 1967, *Proc. Roy. Soc.A.* 301, pp. 39-45.
3. Shirk, E.K., and Price, P.B.: 1978, *Astrophys.J.* 220, pp. 719-733.
4. Israel, M.H., Klarmann, J., Love, P.L., and Tueller, J.: 1979, *Proc. 16th Int. Cosmic Ray Conf.*, Kyoto 12, pp.65-69.
5. Fowler, P.H., Alexandre, C., Clapham, V.M., Henshaw, D.L., O'Sullivan, D., and Thompson, A.: 1977, *Proc. 15th Int. Cosmic Ray Conf.*, Plovdiv 11, pp. 165-173.
6. Cameron, A.G.W.: 1973, *Space Sci. Rev.* 15, pp. 121-146.
7. Price, P.B., and Shirk, E.K.: 1975, *Proc. 14th Int. Cosmic Ray Conf.*, Munich 1, pp. 268-272.
8. Fowler, P.H.: 1977, *Nucl. Instr. and Meth.* 147, pp. 183-194.
9. Cassé, M., Goret, P., and Cesarsky, C.J.: 1975, *Proc. 14th Int. Cosmic Ray Conf.*, Munich 2, pp. 646-650.
10. Ohnishi, T.: 1978, *Astrophys. Space Sci.* 58, pp. 149-165.
11. Steinberg, E.P., and Wilkins, B.D.: 1978, *Astrophys.J.* 223, pp.1000-1014.
12. Schramm, D.N., and Fowler, W.A.: 1971, *Nature* 231, pp.103-106.
13. Blake, J.B., and Schramm, D.N.: 1974, *Ap. Space Sci.* 30, pp.275-290.
14. Wefel, J.P., Schramm, D.N., and Blake, J.B.: 1977, *Astrophys. Space Sci.* 49, pp.47-81.